Tellus (2002), 54A, 159–174
Printed in UK. All rights reserved

TELLUS
ISSN 0280–6495

Thermohaline circulation sensitivity to intermediate-level anomalies

By VINCENZO ARTALE[1]*, SANDRO CALMANTI[2] and ALFONSO SUTERA[3], [1]*ENEA, Centro Ricerche Energia, Casaccia, Rome, Italy;* [2]*Dipartimento di Fisica, Università di Roma "La Sapienza", Italy;* [3]*Dipartimento di Fisica, Università di Roma "La Sapienza", Italy*

(Manuscript received 25 January 2001; in final form 31 July 2001)

ABSTRACT

A two-dimensional Boussinesq ocean model has been used to investigate the effect of intermediate-level thermal and saline anomalies on the known multiple equilibria structure of the thermohaline circulation. These anomalies are taken as a crude representation of the Mediterranean outflow in the Atlantic Ocean. The associated perturbation drives the system towards an overturning which resembles the present average Atlantic thermohaline circulation. The sensitivity to the depth at which the anomaly is placed is also investigated. We found that near-surface anomalies are more efficient in affecting the structure of the equilibria.

1. Introduction

The North Atlantic Ocean transports large amounts of heat polewards, thus contributing to the current climate state. However, the analysis of climate records shows that this transport may change dramatically on a short timescale (Boyle and Keigwin, 1987). Broecker et al. (1985) have suggested that a rapid switching of the North Atlantic thermohaline circulation may be the cause of the termination of the Younger Dryas episode. The timescale involved was as short as a few decades (Dansgaard, 1989). As a rule, an abrupt change in the dynamical behaviour of a system calls for non-linear interactions among its state variables. As suggested by Broecker et al. (1990), such a set of couplings may deeply involve ocean salinity.

Modeling studies suggest that the North Atlantic ocean circulation may support multiple equilibria, which is a main feature that a non-linear system generally shows. Multiple equilibria have been considered for modeling the 100 ky (1 ky = 1000 years) glaciation cycle which occurred during the Pleistocene (Sutera, 1981), the atmospheric blocking phenomenon (Charney and De Vore, 1979), and as a description of other phenomena of climatic relevance. Studying ocean dynamics, Bryan (1987) has discussed multiple equilibria within a three-dimensional primitive equations ocean model. Holland and Bryan (1993a) have also shown the existence of two equilibria states using mixed boundary conditions at the ocean–atmosphere interface. Two-dimensional meridional-plane models show a similar behaviour (Marotzke et al., 1988).

As illustrated by the pioneering work of Stommel (1961), the interplay between salt and heat gradients is the main contributor to the possible existence of multiple equilibria in ocean circulation models. Therefore, it is mandatory to consider the effect of all the water sources which may contribute to establish the observed ocean water salt and heat budget. For example, Weijer

* Corresponding author.
Via Anguillarese 301, 00060, Santa Maria di Galeria (Roma), PO Box 2400, Italy.
e-mail: artale@casaccia.enea.it

et al. (1999) discuss the effect of lateral forcing on stabilizing certain equilibria of the meridional overturning circulation of the Atlantic ocean. They find that the northern pole-to-pole (NPP) circulation is favoured by the presence of a particular formulation of the lateral heat and salt fluxes. These fluxes are interpreted as the interbasin exchange at the southern boundary through the Aghulas leakage. Weijer et al. (1999) stress also the role of the vertical structure of the heat–salt fluxes as a major contributor to the strength of the meridional circulation.

An important interbasin exchange of waters takes place at the Straits of Gibraltar. The very warm and saline Mediterranean intermediate waters, which flow into the Atlantic, may play a role in North Atlantic deep water formation and its meridional overturning (Reid, 1979).

Despite the potential role in modifying the large-scale circulation, studies on the oceanic response to variations in the source of Mediterranean waters have been sparse. Stanev (1992) studied the influence of Mediterranean waters on the Atlantic circulation at an intermediate depth. However, he did not account for the variability in the composition of the upper 1000 m of the ocean. Rahmstorf (1998) found, integrating a coarse resolution general circulation model, that the North Atlantic thermohaline circulation has a low sensitivity to the inflow of Mediterranean waters. In fact, he observed a small, though noticeable, increase in the strength of the overturning from 16 Sv (without the Mediterranean inflow) to 18 Sv (with the Mediterranean inflow). On the other hand, Hecht et al. (1997) found that the Mediterranean water is crucial in characterizing the thermohaline structure of the North Atlantic. The latter authors used the Community Modeling Effort (CME) North Atlantic model (Holland and Bryan, 1993a,b) and compared experiments performed with and without Mediterranean waters. In particular, an experiment was presented where the exchange of waters at Gibraltar was diagnosed from an independent model of the Mediterranean circulation (Roussenov et al., 1995). The resulting long-term thermohaline circulation was maintained only if Mediterranean outflow was included. Presumably, this occurred because the enhanced vertical salinity gradient associated with the Mediterranean water sustains a continuous deep-water formation in the northern part of the basin. OGCM's experiments, such as those of Rahmstorf (1998) or Hecht et al. (1997), have brought up major findings giving a fairly good picture of the actual Atlantic meridional circulation. However, it would be difficult to exhaust the effect of Mediterranean water on the Atlantic thermohaline circulation only from the analysis of OGCM's experiments. In fact, this may be an incomplete investigation regarding the presence of multiple equilibria and their dynamical content. The purpose of the present paper is to contribute to the understanding of the influence of the warm and salty water inflow in the North Atlantic carried by Mediterranean water in a frame where multiple equilibria exist. In particular we wish to elucidate the effect of different vertical distributions of internal perturbations in the heat and salt content. We will study the sensitivity of an equatorially symmetric ocean to anomalies that may crudely represent the Mediterranean water inflow at intermediate level.

The paper is organized as follows. A brief overview of the two-dimensional Boussinesq model and of the numerical techniques employed here is given in sections 2 and 3. In section 4 we discuss some standard reference cases, both as a test of the numerical scheme and as a basis for further investigations. In sections 4.1 and 4.2 we discuss the effect of internal anomalies on the dynamics of the model. Conclusions and discussions are presented in section 5.

2. Model formulation

The Boussinesq equations for a two-dimensional (y, z) layer of fluid in a non-rotating rectangular basin have been widely used as a first approximation of the zonally averaged thermohaline circulation [see, for instance, Dijkstra and Molemaker (1997), Vellinga (1996), Cessi and Young (1992), Quon and Ghil (1992) and Thual and McWilliams (1991) and references therein]. The equations are given in the appendix. However, here we wish to discuss shortly the implication of using a linear equation of state and the motivation of some of our parameter choices.

The buoyancy forcing

$$B = \frac{\partial}{\partial y^*}(T^* - \lambda S^*)$$

in eq. (A6) (where the asterisks represent non-dimensional quantities) is due to the assumption that a linear equation of state for sea-water holds:

$$\rho = \rho_0[1 - \alpha(T - T_0) + \beta(S - S_0)]. \quad (1)$$

This is commonly used, as the papers already quoted show. However, non-linearities in the equation of state may sometimes have significant effect on the dynamics. In fact, when the full non-linear equation of state of sea-water is considered, the mixing of water masses having different salinity and temperature, but the same density, may produce a water mass which is denser than the original ones. This mechanism is usually referred as *cabbeling* (Pickard and Emery, 1990). It could play a role in our study. In fact, we are going to investigate the effect of an input of water mass whose temperature and salinity are different from the values found elsewhere, while its density is the same as that of the water present at the specified level at which it is injected in the basin. However, it is known that cabbeling becomes an efficient process only at low temperatures. Numerical model studies of the spreading of Mediterranean water in the North Atlantic (e.g. Gerdes et al., 1999) show that cabbeling plays only a marginal role, probably because the temperature involved is quite high. Thus, eq. (1) appears to be appropriate for our study.

In motivating our parameter's choice, we observe that a two-dimensional model of the thermohaline circulation is an over-simplification of the real ocean dynamics. The external temperature and salinity forcings are only balanced by the viscosity. The use of a parameter setting corresponding to a realistic geometry ($L \sim 10^7$ m, $D \sim 5 \times 10^3$ m) and to the typical values of the viscosity and the tracer diffusivity ($A_H = 2.5 \times 10^5$ m^2 s^{-1}, $K_H = 10^3$ m^2 s^{-1}), would lead to unrealistically high meridional velocities. In the real ocean, the prevailing balance is geostrophic. This would allow the use of the above-mentioned realistic values. In overcoming this limitation a common practice (in the two-dimensional formulation) is to parameterize the zonal pressure gradients resulting from a given meridional forcing on the basis of OGCM's outcomes (Wright and Stocker, 1991). Alternatively, it is possible to arbitrarily lower the Rayleigh number (Weijer et al., 1999) to a value such that a reasonable transport is obtained. As demonstrated by Vellinga (1996), in the latter case the structure of the equilibria of the thermohaline circulation is not greatly affected by the details of the momentum balance. Weijer and Dijkstra (personal communication, paper submitted to *J. Marine Res.*) showed that the physics of thermohaline processes in a two-dimensional model has its three-dimensional counterparts when the effect of earth's rotation is taken into account. In other words the mechanism destabilizing the symmetric circulation is the same both in two-dimensional and three-dimensional dynamics while, for the two formulations, a different parameter setting is required. Thereby, we choose the second approach which also turns out to be easily implemented. In particular, in our work, we adopted the same parameter values as those of Vellinga (1996, see Table 1).

2.1. Internal anomalies

Internal anomalies in the heat and salt content are introduced in the model equations as a crude representation of the mediterranean outflow. In the *free* case, the ocean exchanges heat and salt only through its upper surface, implying that the ocean–atmosphere interface is the only source of energy. In the *forced* case we have an additional source of potential energy:

$$\frac{\partial T}{\partial t} + J(T, \psi) = Pr^{1/2}\frac{\partial^2 T}{\partial y^2} + r_d Pr^{1/2}\frac{\partial^2 T}{\partial z^2} + \theta_i s(y, z), \quad (2)$$

$$\frac{\partial S}{\partial t} + J(S, \psi) = Pr^{1/2}\frac{\partial^2 S}{\partial y^2} + r_d Pr^{1/2}\frac{\partial^2 S}{\partial z^2} + \sigma_i s(y, z). \quad (3)$$

Here σ_i and θ_i are the amplitude of the temperature and salinity anomalies, $s(y, z)$ is a shape function, which we set as:

$$s(y, z) = \frac{1}{A_0}\exp\left(-\frac{(y - y_0)^2}{W^2}\right)\exp\left(-\frac{(z - z_0)^2}{H^2}\right), \quad (4)$$

where z_0 is the height of the anomaly from the bottom of the basin, y_0 is the latitude at which the anomaly is centred, and H and W are the vertical and meridional extensions of the anomaly. A_0 is a normalization factor such that

$$\int_\Omega s(y, z)\, d\Omega = 1.$$

Table 1. *List of model parameters. The internal anomaly scale is given in eq. (6)*

Parameter	Value	
Dimensional parameters		
g	$9.8\ \mathrm{m\ s^{-2}}$	Gravity
α	$10^{-4}\ ^{\circ}\mathrm{C}^{-1}$	Thermal expansion
β	$3 \times 10^{-4}\ \mathrm{psu}^{-1}$	Haline expansion
T_0	12.5°C	Reference temperature
$\bar{T}$	25°C	Equator to pole temperature difference
S_0	36 psu	Reference salinity
$\bar{S}$	3.2 psu	Equator to pole salinity difference
k_H	$10^5\ \mathrm{m^2\ s^{-1}}$	Horizontal diffusivity
k_V	$10^{-1}\ \mathrm{m^2\ s^{-1}}$	Vertical diffusivity
ν_H	$4.7 \times 10^4\ \mathrm{m^2\ s^{-1}}$	Horizontal viscosity
ν_V	$4.7 \times 10^{-2}\ \mathrm{m^2\ s^{-1}}$	Vertical viscosity
L	10^6 m	Basin length
D	10^3 m	Basin depth
$\bar{\sigma}_i$	$2.2 \times 10^{-7}\ \mathrm{psu\ s^{-1}}$	Internal anomaly
Dimensionless parameters		
Ra	5×10^3	
Pr	2.25	
δ	10^{-3}	
r_v, r_d	1	
λ	0.38	

The salt and heat anomalies do not affect directly the stability of the water column, since we assume the following linear equation:

$$\theta_i = \lambda \sigma_i, \tag{5}$$

where λ is defined in the Appendix. From now on, we only make explicit mention of the parameter σ_i, since θ_i can be obtained from eq. (5). A direct estimate of σ_i on the basis of data is a difficult task, especially when a two-dimensional model is considered. In fact, it is not clear how to parameterize the volume over which the internal anomaly is spread. However, the non-dimensional parameter σ_i should be taken as a small value or, at least, comparable to the advection and diffusion terms in the heat–salt equation. Therefore, a study of the response within a range of σ_i values centred around 1 allows a qualitative analysis of the effect of the internal anomaly on the overturning. With a viscous-diffusive timescale

$$\bar{t} = \frac{L^2}{(\nu_H k_H)^{1/2}}$$

and salinity scale $\bar{S}$ (see Appendix and Table 1 for details), a non-dimensional $\sigma_i = 1$ corresponds to the dimensional value:

$$\bar{\sigma}_i = \frac{(\nu_H k_H)^{1/2} \bar{S}}{L^2}. \tag{6}$$

This gives an order of magnitude of $\bar{\sigma}_i \sim 10^{-7}\ \mathrm{psu\ s^{-1}}$. This is sufficiently consistent with a Mediterranean outflow of about 1 Sv (1 Sverdrup $= 10^6\ \mathrm{m^3\ s^{-1}}$) which is spreading in a vein a few hundreds metres thick, a few hundred kilometres wide and travelling northwards for a thousand kilometres (a volume $V \simeq 10^{13}\ \mathrm{m^3}$) (Baringer and Price, 1997).

Also, we wish to investigate the impact of internal anomalies placed at different depths. For this purpose, we will set in eq. (4) the following values:

$$y_0 = 3/4,$$

$$W = H = 3/8,$$

while z_0 takes the following discrete values:

$$z_0 = 3/4; \quad z_0 = 1/2; \quad z_0 = 1/4.$$

The internal sources of heat and salt introduced in eqs. (2) and (3) must be balanced to avoid an unrealistic increase of the integrated heat and salt

content. We are interested in the competition between meridional density gradients due to the surface boundary conditions and those induced by the presence of the internal anomaly. To keep the balance unchanged the following procedure may be considered. Let us subtract uniformly over the first layer at the surface the total amount of tracer added when the internal anomaly is applied. This approach is a reasonable approximation which overcomes the lack of a detailed description of how the internal source is physically balanced. Notice that using this adjustment causes a small change in the surface forcing, which may lead to slight modification in the bifurcation diagram. In particular, it may cause a shift of the value of the bifurcation point. However, as we will explain in more detail later, we calculate the steady states only at discrete intervals of the control parameter. So doing, we are not able to detect such a shift. Thus, within the degree of accuracy we have adopted in describing the bifurcation diagram, the salt–flux adjustment surface does not affect the results.

3. Numerical procedure

Each of the model equations in the Appendix may be written in the general form:

$$\frac{\partial q}{\partial t} = -J(q,\psi) + K_{\mathrm{H}}\frac{\partial^2 q}{\partial y^2} + K_{\mathrm{V}}\frac{\partial^2 q}{\partial z^2}, \tag{7}$$

where q may be ξ, T or S. K_{H}, K_{V} are either the diffusion or the eddy viscosity coefficient. An additional term B (the buoyancy) must be included when the vorticity equation is considered.

Discretization of the model on a rectangular grid leads to the solution of a system of ordinary differential equations:

$$\dot{\boldsymbol{q}} = D\boldsymbol{q} - J(\psi)\boldsymbol{q}. \tag{8}$$

The vector $\boldsymbol{q}$ represents the values of ξ, T and S at each grid point; D is a linear operator representing diffusion and $J(\psi)$ is the finite difference expression for the Jacobian. In solving eq. (8) we adopted a semi-implicit alternate direction method (ADI; Varga, 1962) for the linear terms, as if we were solving a heat equation. The advective terms may be thought as a further local source (or sink) for T, S or ξ, which is numerically treated following the Arakawa (1966) formulation of the Jacobian.

The stream function is calculated each time step with a simple inversion of the laplacian-employing ADI method. The use of a semi-implicit time scheme allows a timestep $\Delta t = 1/10$ day. The ADI method also reduces computer time. The grid has 125×25 points in latitude and height, respectively.

4. Results

Most studies related to the problem of two-dimensional thermohaline circulation focus on the role of external boundary conditions. Instead, we will consider the effect anomalies. However, a comparison with previous results (in particular with those of Vellinga, 1996) achieves a twofold goal. First, we can test the numerical scheme we have employed. Secondly, it allows an overview of what we call here the *free* circulation, i.e. the circulation generated by the external forcing only. To study the structure of the bifurcation diagram, we have followed the procedure of Quon and Ghil (1992). It may be outlined as follows. Starting from an homogeneous ocean at rest, we applied fixed surface temperature and salinity profiles until the system reaches a steady state. It turns out that this state is symmetric about the center of the basin (a steady state is reached when $\mathrm{d}E/\mathrm{d}t = 0$, E being the basin integral of kinetic energy). For this steady state, the salinity flux at the surface is diagnosed, and, when further integrations are performed, *mixed boundary conditions* are applied, namely:

$$T(y,0) = \cos(2\pi y), \quad \frac{\partial S}{\partial z}(y,0) = \sigma_{\mathrm{e}} g(y), \tag{9}$$

where $g(y)$ is the surface salinity gradient diagnosed at the end of the spin up integration, while σ_{e} is the control parameter that measures the strength of the salinity forcing. The state of the system is traced by looking at the domain average vorticity $\langle\xi\rangle$.

Following the nomenclature used in literature, the NPP (SPP) steady states are those characterized by negative (positive) values of the averaged vorticity. Symmetric TH solutions have zero averaged vorticity. The known bifurcation diagram of this system is obtained when our model is considered. For low values of the control parameter only symmetric solutions are found to be stable steady states. In fact, for any small perturbation to the

initial condition, the numerical solution converges to a symmetric steady state. For higher enough values of the control parameter (i.e. stronger enough surface forcing) the advective feedback (described, for example, in Dijkstra and Molemaker, 1997) sets in. The symmetric circulation looses its stability through a supercritical pitchfork bifurcation. Two branches of mutually symmetric stable equilibria (NPP and SPP) show up. Unfortunately, since we are solving prognostic equations, we are not able to follow easily the unstable branches.

Figure 1 shows the bifurcation diagram obtained with the symmetric setup. We note that, in spite of the slightly different formulations of the models, the bifurcation diagram resembles quite well that obtained by Vellinga. The pitchfork bifurcation occurs at a value σ_p of the control parameter in between $\sigma_e = 0.65$ and $\sigma_e = 0.7$. By interpolating through

$$\sigma_e = \sigma_p + A\langle\xi\rangle^2 \tag{10}$$

(as similarly done by Quon and Ghil, l.c.) we have $\sigma_p = 0.69$. Vellinga, using a branch continuation technique, obtained $\sigma_p = 0.67$, which is in quite good agreement with our value. We notice that the two models differ substantially in the way they remove unstable vertical stratification. Vellinga employs an implicit vertical diffusion scheme to parameterize convective processes, since the hydrostatic approximation is used there. On the contrary, we explicitly remove unstable vertical stratification by means of a net vertical mass flux. The close agreement between the values of σ_p found with the two models suggests that such a different formulation plays only a minor role. For reference, in Fig. 2 a few examples are shown of the different types of equilibria which are found below and above the bifurcation.

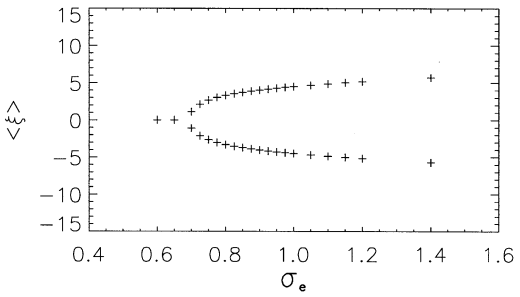

Fig. 1. Bifurcation diagram obtained with the symmetric surface forcing in absence of internal anomalies. The basin-averaged vorticity $\langle\xi\rangle$ is non-dimensional and the control parameter σ_e represents the strength of the surface freshwater forcing.

4.1. *Imperfect bifurcation diagram*

Starting from each steady state on the symmetric bifurcation diagram we added an internal perturbation and integrated the system forward in time until a new equilibrium was found. The presence of an internal anomaly, although not affecting the density, forces an advective feedback towards the northern hemisphere. In fact, the temperature anomalies are partially damped by the strong restoration at the surface. On the other hand, salinity anomalies are advected northwards, producing an overall enhancement of the northern convection cell.

In the jargon of the imperfection theory (Dijkstra, 2000), a symmetric system (i.e., the basin with symmetric surface forcing) is slightly perturbed to give preference to certain dynamical behaviours. We shall call *imperfect* bifurcation diagrams those obtained with the same kind of surface boundary condition, as in the previous section when an internal anomaly is further applied.

When the internal perturbation is applied at $z_0 = 3/4$, starting from a steady state on the stable TH branch (the symmetric steady states before the pitch-fork), a weak NPP state is reached [first two points in Fig. 3(a)]. Likewise, if a perturbation is applied to an NPP state, only small changes about the unperturbed values of both averaged vorticity and maximum overturning are found [Figs. 3(a) and 3(b)]. Consider now a steady state on the SPP branch just above the pitchfork. If the surface forcing is weak, the advective feedback is no longer able to maintain an SPP circulation when the internal anomaly is applied. In fact, even if we start from an SPP state, the internal anomaly causes a reversal of the circulation. It turns out that for values of σ_e slightly above σ_p, only NPP-like steady states exist. SPP steady states appear only when the surface forcing is strong enough to sustain the advective feedback towards the southern hemisphere. Looking at the strength of overturning [Fig. 3(b)] we observe that NPP and SPP steady states could not be separated on the symmetric bifurcation diagram because they were

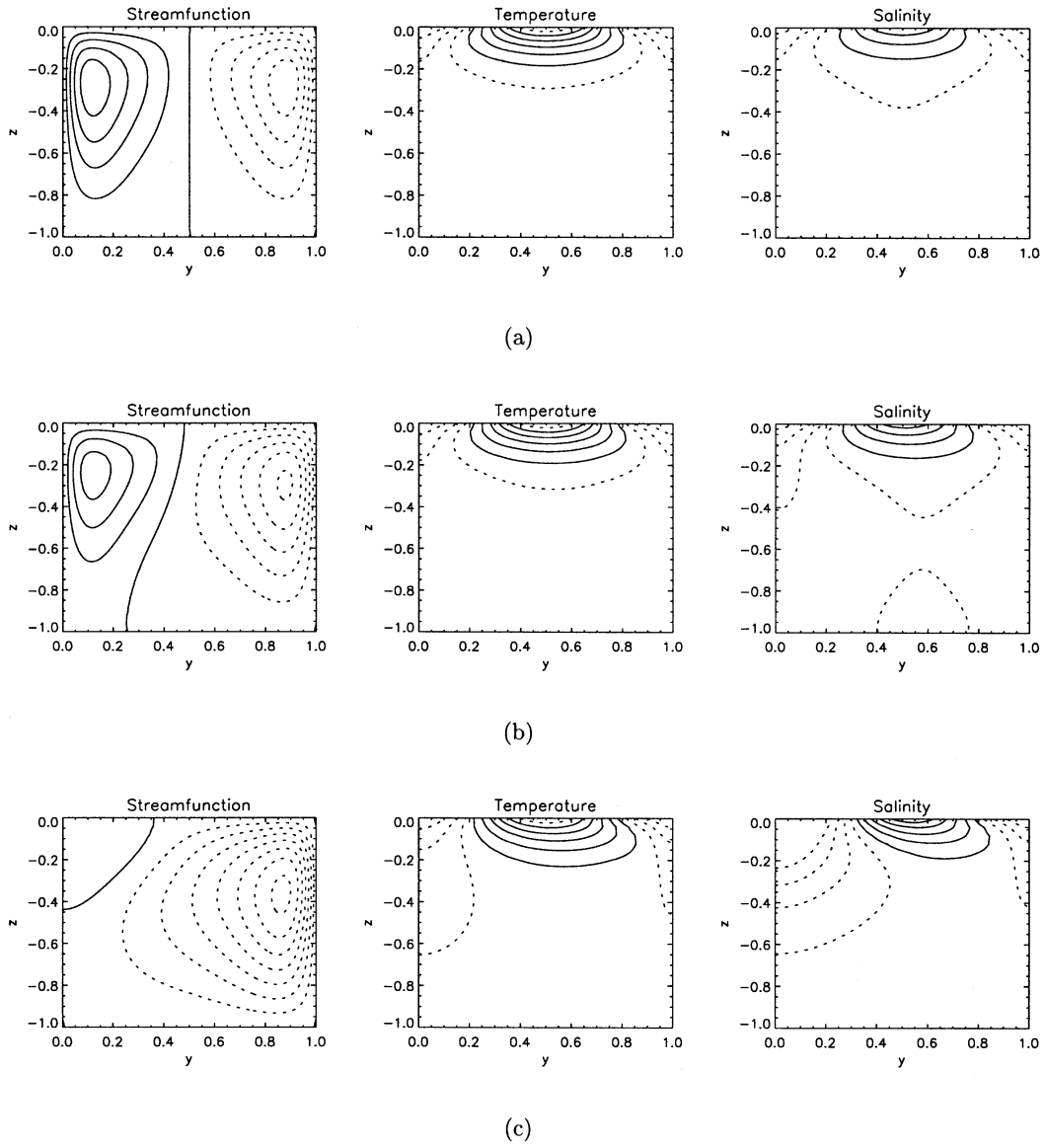

Fig. 2. Streamfunction, temperature and salinity obtained with mixed boundary condition and three different values of σ_e. (a) $\sigma_e = 0.6$, before the pitchfork; (b) $\sigma_e = 0.7$; (c) $\sigma_e = 1.0$. Contour values are non-dimensional. Continous (dotted) lines correspond to positive (negative) values. Isolines spacing is 1 for the streamfunction and 0.1 for temperature and salinity.

essentially the same equilibrium reflected about the equator. Instead, for the *imperfect* system, SPP steady states are weaker. Note that, compared with the symmetric setup, for some values of the internal anomaly a small increase in the overturning of a few percent is found. This is consistent with the results of Rahmstorf (1998), who obtained about 10% difference between experiments with and without the Mediterranean outflow. With our approach, the unstable steady states can not be reached. However, an inversion point can be guessed on the *new* SPP branch leading to TH-like

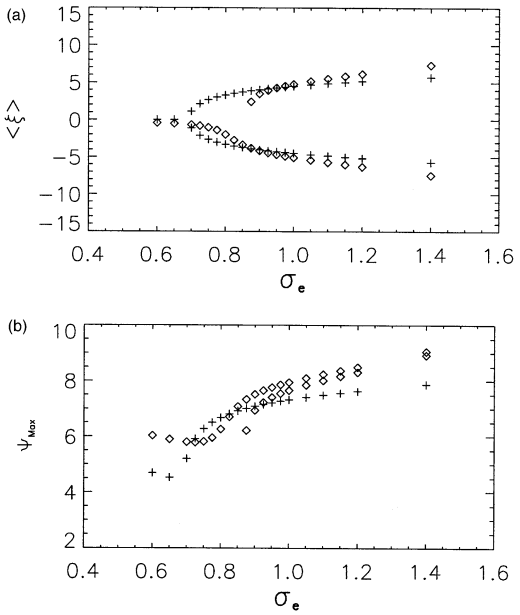

Fig. 3. Comparison between the bifurcation diagrams obtained with the symmetric setup (crosses) and with an internal anomaly of strength $\sigma_i = 0.5$ (diamonds). (a) Stationary states are traced by means of averaged vorticity; (b) maximum absolute value of the streamfunction. Values are non-dimensional.

unstable steady states. In Fig. 4 we compare NPP steady states at $\sigma_e = 1.0$, $\sigma_i = 0.5$ and NPP states at $\sigma_e = 1.0$, $\sigma_i = 0.0$ (i.e. without internal anomaly). This means that we are comparing two NPP states with the advective feedback already at work. The difference between the two solutions shows how this feedback is favoured in the presence of an internal anomaly. A stronger temperature gradient in the most northern region shows up at the surface in presence of the Mediterranean outflow. This allows a partial damping of the temperature anomaly, while the salinity anomaly is more easily advected northwards, thus determining in a net positive density anomaly near the sinking region. Consistently, the increased surface density enhances the meridional overturning, as the structure of the stream function anomaly shows.

When we consider the effect of the anomaly on SPP states (Fig. 5), the surface temperature gradients are much weaker, since warm waters are advected towards regions of higher surface temperatures. Density anomalies at the surface in the region of deep convection are weaker because this region is less affected by the advection of salt anomalies. Thus, we get a smaller increase in the overturning when it is compared to the one we obtained for the NPP state. Consistently, deep waters are, on average, weakly affected by the salinity anomaly which is, in this case, less involved in the process of deep water formation.

4.2. Sensitivity experiments

In the previous section we have shown that, in the presence of a particular internal anomaly, only one steady state (NPP-like) exists if σ_e is close to the bifurcation point of the symmetric setup. In climate studies, a question might arise about the effect of changes in the strength of the internal anomaly. Such changes have been suggested to take place in the North Atlantic because of anthropogenic forcing applied to the Mediterranean sea (exploitation of the ground and river water resources). More realistically, changes can occur as a consequence of the natural variability of climate affecting the E–P balance in the Mediterranean Sea. Figure 6 shows the bifurcation diagrams obtained when the strength of the internal anomaly is increased. It shows that the limit point on the TH-SPP branch is shifted to higher values of the control parameter σ_e. This behaviour is consistent with the statement that internal anomalies, like that described in eq. (4), lead to a preference for the advective feedback towards the North. Increasing the internal anomaly, then, requires a stronger surface forcing to maintain an SPP circulation. Let us denote as Δ the distance (with respect to the control parameter σ_e) between the original pitchfork bifurcation point and the inversion point on the *imperfect* TH-SPP branch. Figure 7 (solid line) shows Δ as a function of σ_i (i.e., the intensity of the internal anomaly). We can not calculate the limit point exactly, because we are computing steady states at discrete values of the internal forcing. However, we can place the limit point in between the value of σ_e corresponding to the first point on the SPP branch and the closest value of σ_e corresponding to a steady state on the NPP branch. A refinement of the resolution would imply the calculation of new points on the bifurcation diagram and the successive computation of the perturbed equilibrium. This is computationally costly and is not likely to add further enlightment to the analysis.

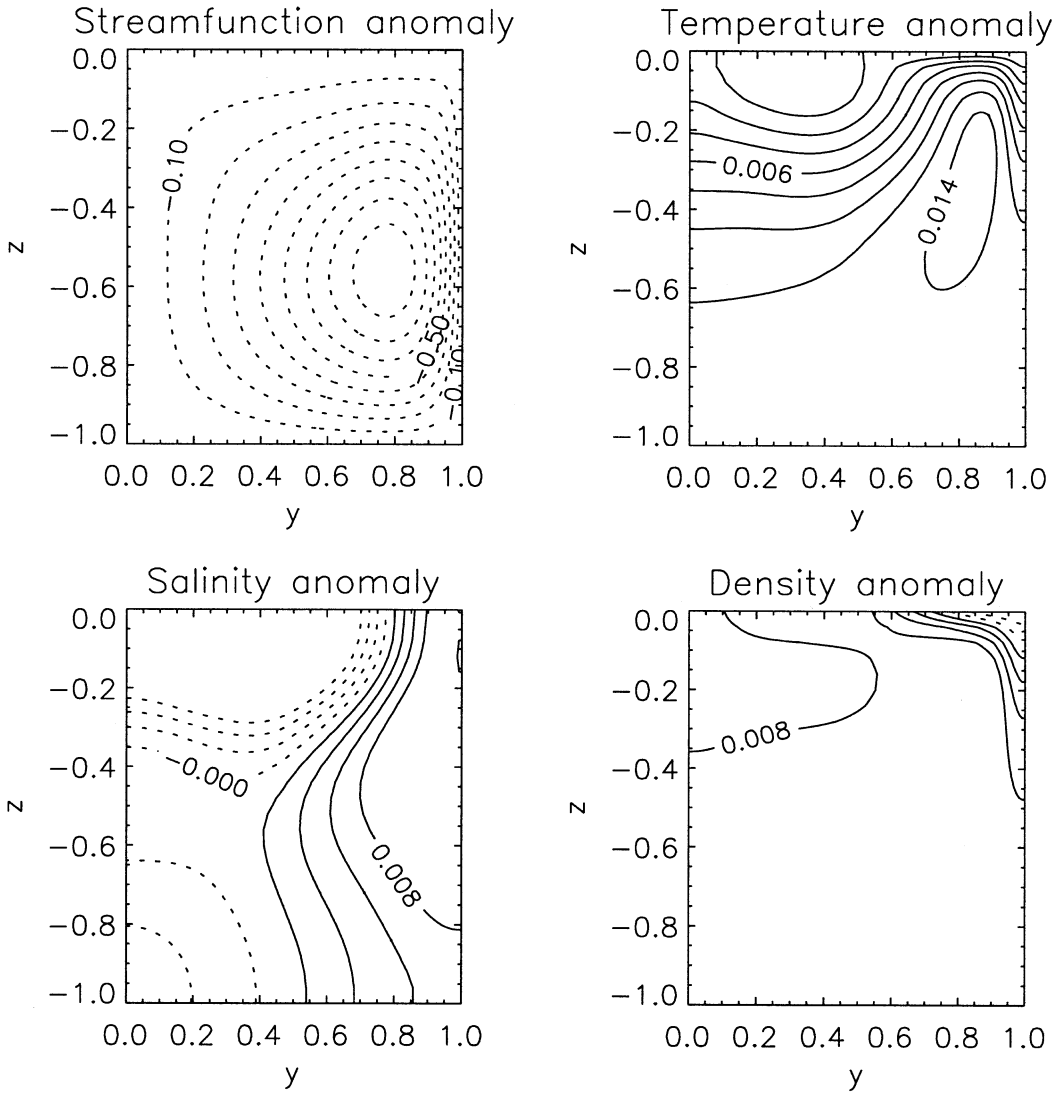

Fig. 4. Streamfunction, temperature, salinity and density difference between NPP state at $\sigma_e = 1.0$, $\sigma_i = 0.5$ and the corresponding equilibrium obtained with the symmetric setup ($\sigma_e = 1.0$, $\sigma_i = 0.0$). The internal anomaly in the *perturbed* circulation is placed at $z = 3/4$. Continous (dotted) lines correspond to positive (negative) values. The spacing of the isolines is 0.1 for the streamfunction anomaly, and 0.002 for the temperature, salinity and density anomaly.

Instead, it is interesting to compare the impact of internal anomalies placed at different levels. We can use the same procedure described before that has been used to build the imperfect bifurcation diagram, when the internal anomaly is placed at $z_0 = 1/2$ and at $z_0 = 1/4$. The complete bifurcation diagrams are not shown because they look quite similar to Fig. 6. However, the dependence of Δ on σ_i is shown in Fig. 7 (dashed and dotted lines). For low values of σ_i the shift of the inversion point is not detectable. As the strength of the anomaly is increased, the impact on the structure of the equilibria appears to be weaker if the anomaly itself is placed at a lower depth. This occurrence

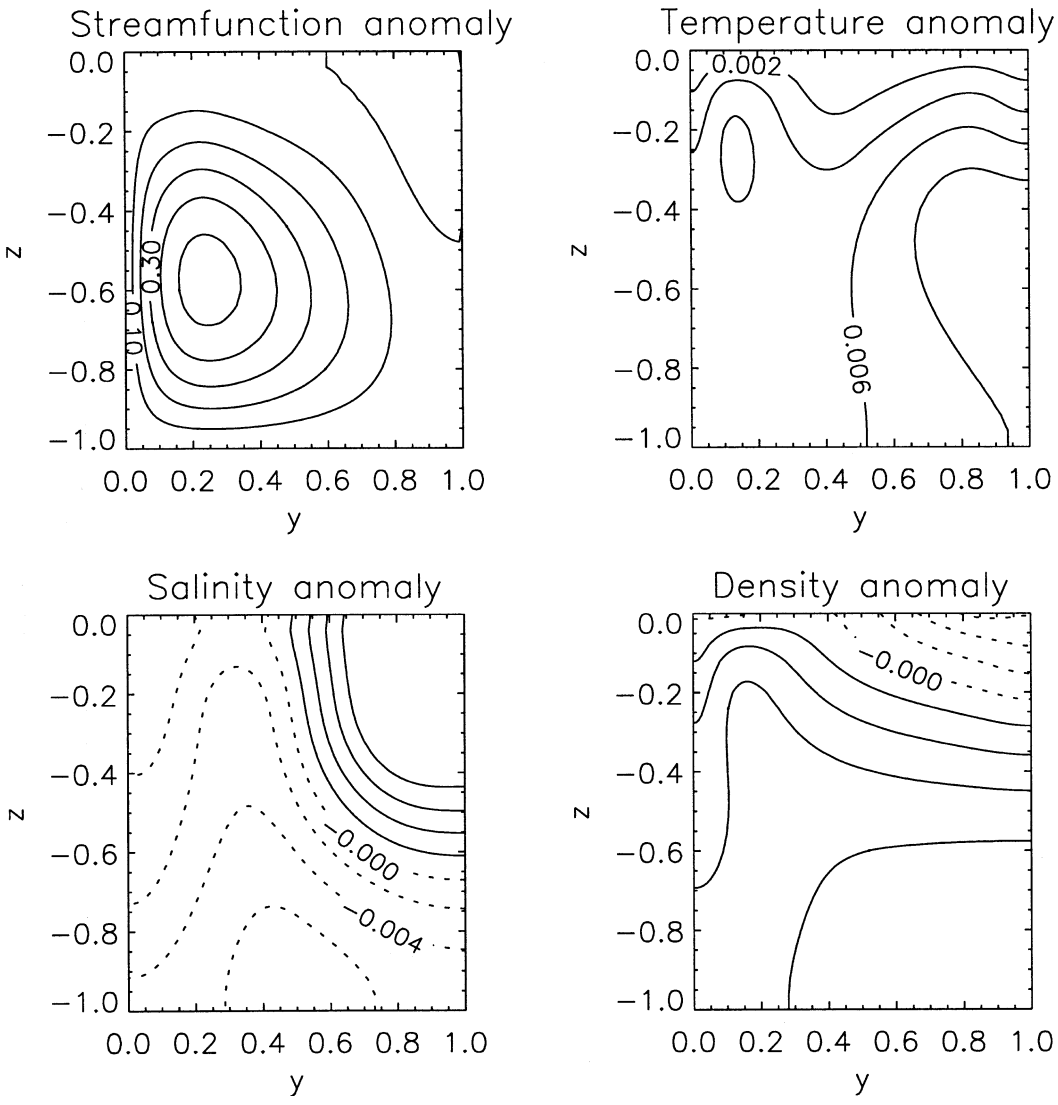

Fig. 5. As Fig. 4, but for an SPP circulation.

can be accounted as follows. When the anomaly is placed in the upper layers, the mechanism responsible for damping temperature anomalies while enhancing salinity anomalies is more efficiently excited. On the contrary, when the anomaly is placed in a deeper layer, the damping on temperature is weaker. Thus, salinity and temperature anomalies partially compensate. A weaker surface forcing is therefore sufficient to involve the southern hemisphere with the advective feedback. The different behaviour of the system with internal anomalies placed at different depths is illustrated in Figs. 8 and 9. The weaker temperature gradients at the surface found in the case of an anomaly placed at the lowest depth means a weaker damping of the anomaly itself. Thus a lower increase in density at the surface and consequently a weaker anomaly in the strength of the overturning has to be expected.

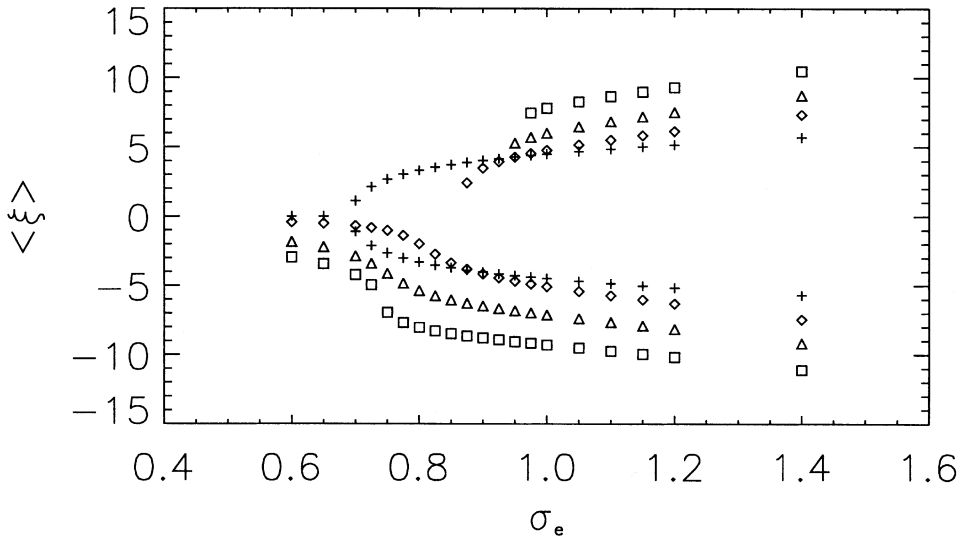

Fig. 6. Bifurcation diagrams corresponding to different strength of the internal anomaly: symmetric setup (crosses); $\sigma_i = 0.5$ (diamonds); $\sigma_i = 2.5$ (triangles); $\sigma_i = 5.0$ (squares).

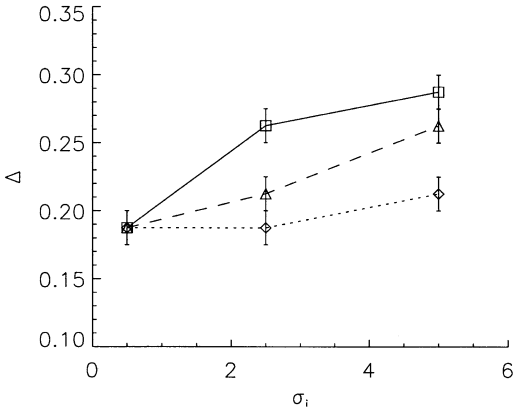

Fig. 7. The interval Δ between the pitchfork bifurcation obtained with the symmetric setup and the limit point on the SPP branch as a function of the strength of the internal anomaly. The dependence is shown for the internal anomaly centered at different heights: $z_0 = 3/4$ (squares); $z_0 = 1/2$ (triangles); $z_0 = 1/4$ (diamonds).

5. Conclusions

Far from being exhaustive, this work raises a set of questions concerning both ocean modeling, and more generally the study of large-scale climate changes. We have shown that the presence of intermediate level anomalies resembling the structure of the Mediterranean outflow in a two-dimensional model of the Atlantic thermohaline circulation has a significant impact on the dynamics of the basin. In fact, the symmetry of the system is lost and an asymmetric NPP circulation is preferred with respect to SPP steady states. The present work shows that care must be taken when interpreting the outcome of OGCMs if a complete dynamical description of the system is not known. For example, consider the result of Rahmstorf, who inferred, from the integration of a course resolution OGCM, a small impact of the Mediterranean Water on the Atlantic thermohaline circulation. Our results support this statement, but we have shown that it may not be a complete assessment of the role of the Mediterranean Sea. On the other hand, Hecht et al. (1997) found a strong overturning to be stable only in presence of a realistic Mediterranean outflow. Also in this case they could not produce a complete dynamical description of the system. With the present paper we suggest a synthesis between the two points of view, in which the Mediterranean intermediate water has a slight influence on the strength of the overturning and a considerable impact on the preference for an NPP circulation. In fact, a general occurrence of our model, in the presence of internal anomalies resembling the Mediterranean outflow, is the appearance of a window of width Δ where multiple

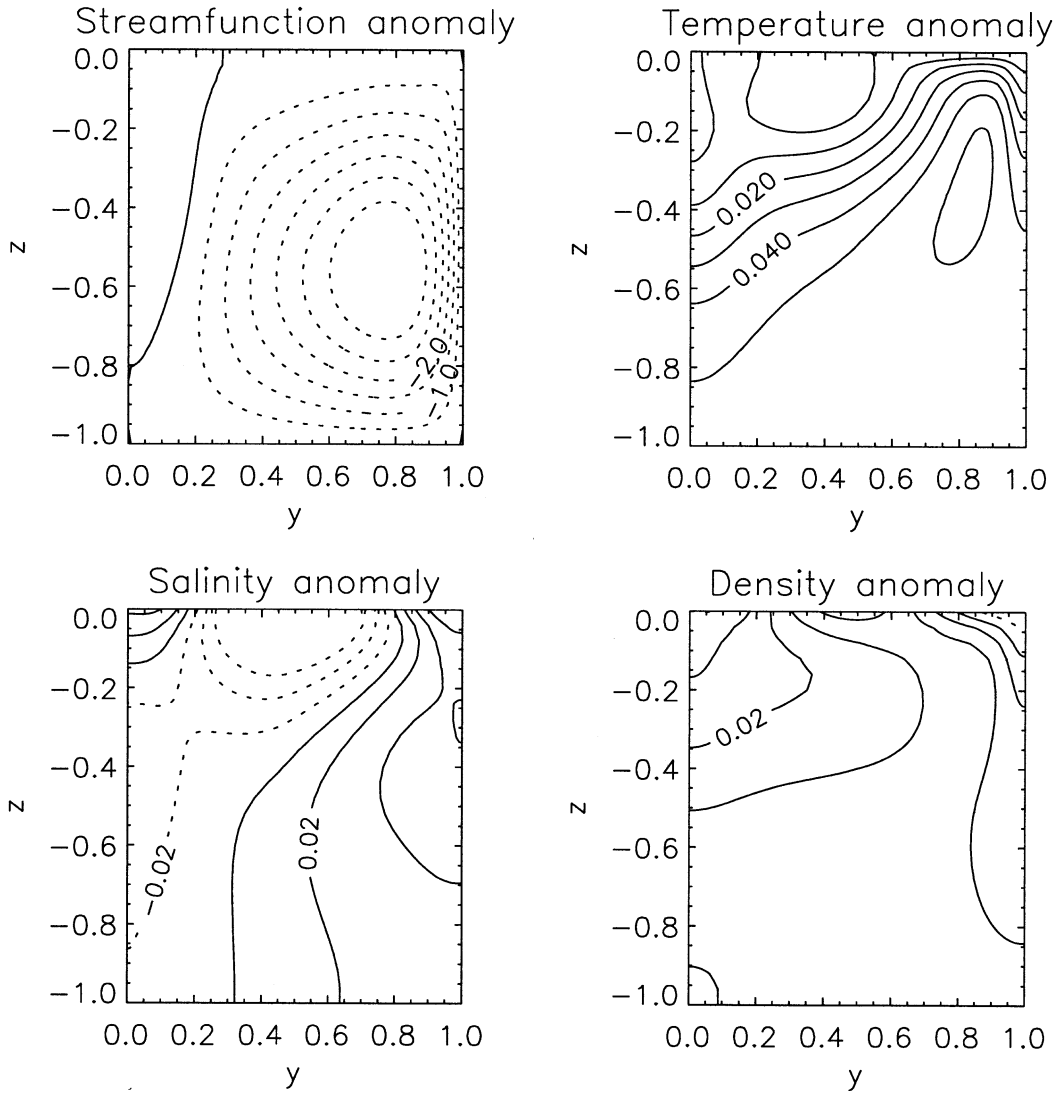

Fig. 8. As Fig. 4, but with $\sigma_e = 0.8$. The spacing of the isolines is 0.5 for the streamfunction anomaly, 0.01 for the temperature anomaly, and 0.02 for the salinity and density anomalies. The value $\sigma_e = 0.8$ was chosen for a clearer visual comparison with the case of anomaly at $z_0 = 1/4$.

equilibria are present in the symmetric case while in the *imperfect* system only NPP states are allowed. Since the present Atlantic thermohaline circulation resembles the NPP state of our simplified model, if the real ocean were perfectly symmetric there would be the possibility of switching between NPP and SPP states. The presence of the Mediterranean outflow seems to stabilize the NPP circulation, preventing the switching at least near the bifurcation point. Clearly, the real ocean has other asymmetries, such as topography, surface and lateral forcing. Other qualitative studies have stressed the impact of such imperfections on the structure of the equilibria (Dijkstra and Neelin, 2000). In these studies, a preference for NPP-like solutions is also found together with a double saddle-node bifurcation on the NPP branch, which leads to the presence of multiple NPP-like

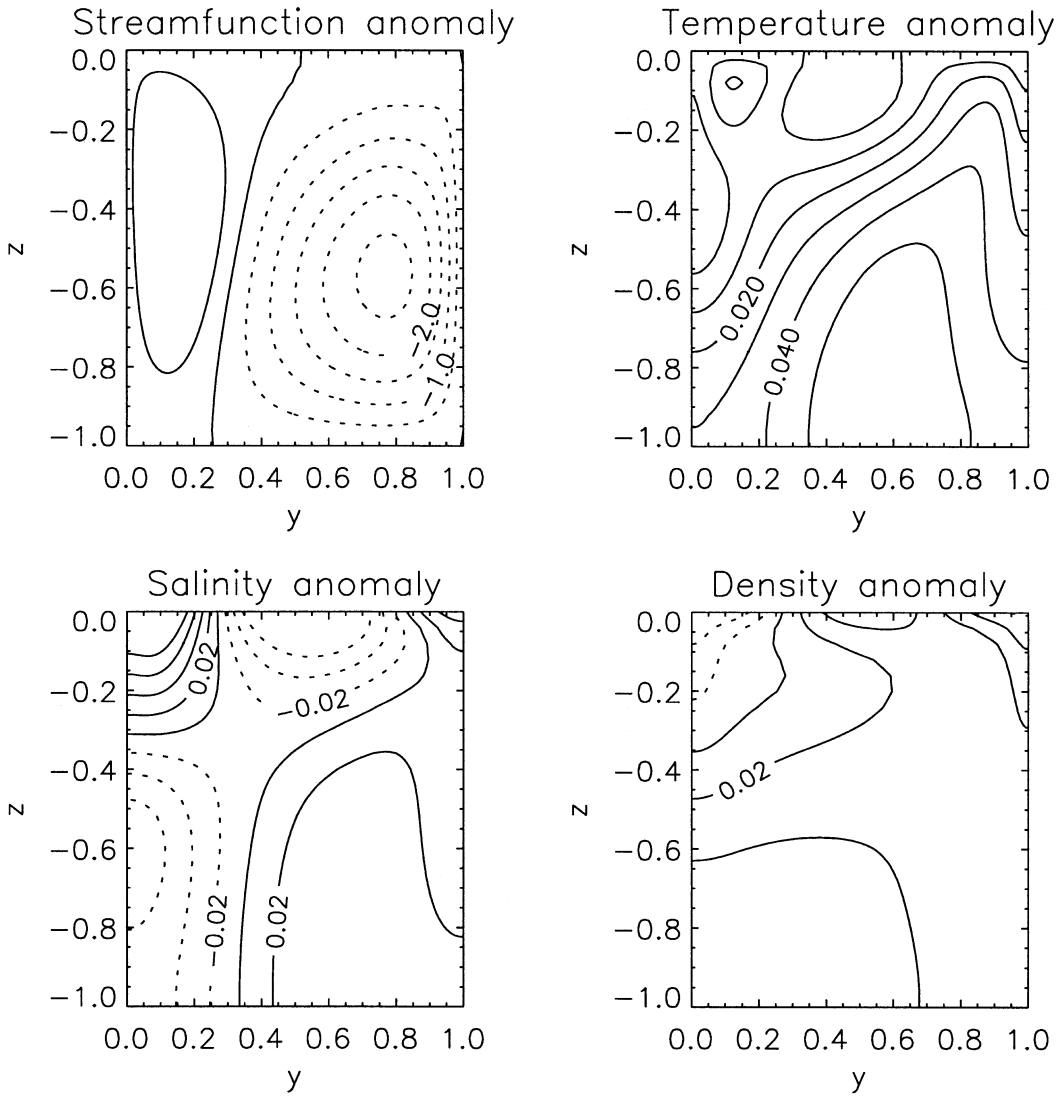

Fig. 9. As Fig. 8, but the internal anomaly is placed at $z_0 = 1/4$.

equilibria. Given that different factors appear to contribute to stabilizing the NPP circulation, an estimate should be sought of the size of the interval Δ. Once an estimate of Δ is given, a major question might be answered: whether the present NPP circulation can switch to an SPP circulation or if other transitions are possible. We have also found a qualitative dependence of the interval Δ on the depth at which the internal anomaly is placed. This behaviour has been explained by means of a simple physical mechanism involving the well known advective feedback. When the anomaly is placed at depth, salinity and temperature anomalies partially compensate each other with a small impact on the structure of the equilibria.

Our study suggests that important qualitative changes in the structure of the equilibria may arise from a poor representation of marginal seas and, in general, of intermediate waters, especially when deep convection processes are involved.

6. Acknowledgments

This research was supported by the UE contracts CLIVAMP (MAS3-CT95-0043) and ASI (CT-99-62). We are grateful to Emanuele Lombardi for his invaluable help in managing the computer facilities that have been employed for this work and to Roberto Iacono for useful comments on the paper. We are also grateful to Henk Dijkstra and Wilbert Weijer for useful discussions while one of us (S.C.) was at IMAU, The Netherlands. We are grateful to two anonymous reviewers who made useful comments and considerably improved the paper.

7. Appendix A

The model equations are:

$$\frac{\partial v}{\partial t} + v\frac{\partial v}{\partial y} + w\frac{\partial v}{\partial z} = -\frac{1}{\rho_0}\frac{\partial p}{\partial y} + \nu_H\frac{\partial^2 v}{\partial y^2} + \nu_V\frac{\partial^2 v}{\partial z^2}, \quad \text{(A1)}$$

$$\frac{\partial w}{\partial t} + v\frac{\partial w}{\partial y} + w\frac{\partial w}{\partial z} = -\frac{1}{\rho_0}\frac{\partial p}{\partial z} + [\alpha(T-T_0) - \beta(S-S_0)]g + \nu_H\frac{\partial^2 w}{\partial y^2} + \nu_V\frac{\partial^2 w}{\partial z^2}, \quad \text{(A2)}$$

$$\frac{\partial v}{\partial y} + \frac{\partial w}{\partial z} = 0, \quad \text{(A3)}$$

$$\frac{\partial T}{\partial t} + v\frac{\partial T}{\partial y} + w\frac{\partial T}{\partial z} = k_H\frac{\partial^2 T}{\partial y^2} + k_V\frac{\partial^2 T}{\partial z^2}, \quad \text{(A4)}$$

$$\frac{\partial S}{\partial t} + v\frac{\partial S}{\partial y} + w\frac{\partial S}{\partial z} = k_H\frac{\partial^2 S}{\partial y^2} + k_V\frac{\partial^2 S}{\partial z^2}, \quad \text{(A5)}$$

where v and w are the meridonal and vertical velocity, p is the pressure, ρ_0 is a reference density value, g the acceleration of gravity, and T and S are the temperature and salinity field. The kinematic viscosity coefficients ν_H, ν_V and the diffusion coefficients k_H, k_V may be considered as a parameterization of small-scale processes and their values are discussed in section 2.

We introduce a streamfunction $\psi(y, z)$ such that $v = \partial\psi/\partial z$ and $w = -\partial\psi/\partial y$. Equations (A1)–(A5) are made non-dimensional by means of the following scaling:

$$y = Ly^*,$$
$$z = Dz^*,$$
$$\psi = UD\psi^*,$$
$$\xi = (U/D)\xi^*,$$
$$t = (L/U)t^*,$$
$$T - T_0 = \bar{T}T^*,$$
$$S - S_0 = \bar{S}S^*,$$

where L and D are the length and depth scales for the basin, respectively; $\bar{T}$ and $\bar{S}$ represent the equator to pole temperature and salinity difference and ξ represents the vorticity:

$$\xi = \frac{\partial w}{\partial y} - \frac{\partial v}{\partial z}.$$

The velocity is scaled by $U = (\nu_H\ k_H)^{1/2}/L$. We get the following non-dimensional equations:

$$\frac{\partial \xi^*}{\partial t^*} + J^*(\xi^*, \psi^*) = Ra\frac{\partial}{\partial y^*}(T^* - \lambda S^*) + Pr^{-1/2}\frac{\partial^2 \xi^*}{\partial y^{*2}} + r_v\, Pr^{-1/2}\frac{\partial^2 \xi^*}{\partial z^{*2}}, \quad \text{(A6)}$$

$$\delta^2\frac{\partial^2 \psi^*}{\partial y^{*2}} + \frac{\partial^2 \psi^*}{\partial z^{*2}} = -\xi, \quad \text{(A7)}$$

$$\frac{\partial T^*}{\partial t^*} + J^*(T^*, \psi^*) = Pr^{1/2}\frac{\partial^2 T^*}{\partial y^{*2}} + r_d\, Pr^{1/2}\frac{\partial^2 T^*}{\partial z^{*2}}, \quad \text{(A8)}$$

$$\frac{\partial S^*}{\partial t^*} + J^*(S^*, \psi^*) = Pr^{1/2}\frac{\partial^2 S^*}{\partial y^{*2}} + r_d\, Pr^{1/2}\frac{\partial^2 S^*}{\partial z^{*2}}, \quad \text{(A9)}$$

where:

$$Ra = \frac{g\alpha\bar{T}DL^2}{k_H\nu_H}, \quad \lambda = \frac{\beta\bar{S}}{\alpha\bar{T}}, \quad Pr = \frac{k_H}{\nu_H},$$
$$\delta = \frac{D}{L}, \quad r_v = \frac{\nu_V}{\delta^2\nu_H}, \quad r_d = \frac{k_V}{\delta^2 k_H}.$$

$J^*(\cdot, \cdot)$ represents the non-dimensional form of the Jacobian:

$$J^*(A,\ B) = \frac{\partial A}{\partial y^*}\frac{\partial B}{\partial z^*} - \frac{\partial A}{\partial z^*}\frac{\partial B}{\partial y^*}.$$

The boundary conditions are:

$$\psi = 0, \quad \xi = 0$$

along the domain's boundaries, and

$$\frac{\partial(S, T)}{\partial n} = 0$$

along the north, south and bottom boundaries ($\partial/\partial n$ indicates the derivative normal to the boundary). At the surface, two different types of boundary condition are used. In non-dimensional form they are:

$$T(y, 0) = S(y, 0) = \frac{1}{2}\cos(2\pi y), \tag{A10}$$

or the mixed boundary conditions

$$T(y, 0) = \frac{1}{2}\cos(2\pi y), \quad \frac{\partial S}{\partial z}(y, 0) = \sigma_e g(y). \tag{A11}$$

$g(y)$ and σ_e are defined in section 4.

REFERENCES

Arakawa, A. 1966. Computational design for long-term numerical integration of the equation of fluid motion: two-dimensional incompressible flow. Part I. *J. Comp. Phys.* **1**, 119–143.

Baringer, M. and Price, J. F. 1997. Mixing and spreading of the Mediterranean outflow. *J. Phys. Oceanogr.* **27**, 1654–1677.

Boyle, E. A. and Keigwin, L. 1987. North Atlantic thermohaline circulation during the past 20,000 years linked to high-latitude surface temperature. *Nature* **330**, 35–40.

Broecker, W. S., Peteet, D. M. and Rind, D. 1985. Does the ocean–atmosphere system have more than one stable mode of operation? *Nature* **315**, 21–26.

Broecker, W. S., Bond, G. and Klas, M. 1990. A salt oscillator in the glacial Atlantic? 1. The concept. *Paleoceanography* **5**, 469–477.

Bryan, F. 1987. Parameter sensitivity of primitive equation ocean general circulation models. *J. Phys. Oceanogr.* **17**, 970–985.

Cessi, P. and Young, W. R. 1992. Multiple equilibria in two-dimensional thermohaline flow. *J. Fluid Mech.* **241**, 291–309.

Charney, J. G. and De Vore, J. 1979. Multiple flow equilibria in the atmosphere and blocking. *J. Atmos. Sci.* **36**, 1205–1216.

Dansgaard, W., White, J. W. C. and Johnsen, S. J. 1989. The abrupt termination of the Younger Dryas climate event. *Nature* **339**, 532–534.

Dijkstra, H. A. and Molemaker, J. 1997. Symmetry breaking and overturning oscillation in the thermohaline driven flows. *J. Fluid Mech.* **331**, 169–198.

Dijkstra, H. A. 2000. *Nonlinear physical oceanography. A dynamical system approach to the large scale ocean circulation and El Niño.* Kluwer Academic Publishers.

Dijkstra, H. A. and Neelin, J. D. 2000. Imperfections of the thermohaline circulation: latitudinal asymmetry versus asymmetric freshwater flux. *J. Climate* **13**, 366–382.

Gerdes, R., Köberle, C., Beckmann, A., Herrmann, P. and Willebrand, J. 1999. Mechanisms for spreading of Mediterranean water in coarse-resolution numerical models. *J. Phys. Oceanogr.* **29**, 1682–1699.

Hecht, M., Holland, W., Artale, V. and Pinardi, N. 1997. North Atlantic model sensitivity to Mediterranean waters. In: *Assessing climate change, results from the model evaluation consortium for climate assessment* (eds. W. Howe and A. Henderson-Sellers), Gordon and Breach Science Publishers, 169–191.

Holland, W. R. and Bryan, F. O. 1993a. Sensitivity studies on the role of the ocean in climate change. In: *Ocean processes in climate dynamics: global and Mediterranean examples* (eds. P. Malanotte-Rizzoli and A. R. Robinson), NATO ASI Series, Kluwer Academic Publishers, Dordrecht, 111–133.

Holland, W. R. and Bryan, F. O. 1993b. Modeling the wind and thermohaline circulation in the North Atlantic Ocean. In: *Ocean processes in climate dynamics: global and Mediterranean examples* (eds. P. Malanotte-Rizzoli and A. R. Robinson), NATO ASI Series, Kluwer Academic Publishers, 135–156.

Marotzke, J., Welander, P. and Willebrand, J. 1988. Instability and multiple steady states in a merdional-plane model of the thermohaline circulation. *Tellus* **40A**, 162–172.

Pickard, G. L. and Emery, W. J. 1990. *Descriptive physical oceanography*, 5th edn, Pergamon Press.

Quon, C. and Ghil, M. 1992. Multiple equilibria in thermosolutal convection due to salt–flux boundary condition. *J. Fluid Mech.* **245**, 446–483.

Rahmstorf, S. 1998. Influence of Mediterranean outflow on climate. *EOS (Transactions, American Geophysical Union)* **79**, 281–282.

Reid, J. L. 1979. On the contribution of the Mediterranean Sea outflow to the Norwegian–Greenland Sea. *Deep-Sea Res.* **26A**, 1199–1223.

Roussenov, V., Stanev, E., Artale, V. and Pinardi, N. 1995. A seasonal model of the Mediterranean Sea general circulation. *J. Geophys. Res.* **100 C7**, 13,515–13,538.

Stanev, E. V. 1992. Numerical experiment on the spreading of Mediterranean water in the North Atlantic. *Deep-Sea Res.* **39**, 1747–1766.

Stommel, H. 1961. Thermohaline convection with two stable regimes of flow. *Tellus* **13**, 224–230.

Sutera, A. 1981. On stochastic perturbation and long-

term climate behaviour. *Quart. J. R. Met. Soc.* **107**, 137–151.

Thual, O. and McWilliams, J. C. 1991. The catastrophe structure of thermohaline convection in a two-dimensional fluid model and comparison with low-order box models. *Geophys. Astrophys. Fluid Dynam.* **64**, 67–95.

Varga, R. S. 1962. *Matrix iterative analysis.* Prentice-Hall.

Vellinga, M. 1996. Instability of two dimensional thermohaline circulation. *J. Phys. Oceanogr.* **26**, 305–319.

Weijer, W., De Ruijter, W. P. M., Dijkstra, H. A. and Van Leeuwen, P. J. 1999. Impact of interbasin exchange on Atlantic overturning. *J. Phys. Oceanogr.* **29**, 2266–2284.

Wright, D. G. and Stocker, T. F. 1991. A zonally averaged ocean model for the thermohaline circulation. Part I: model development and flow dynamics. *J. Phys. Oceanogr.* **21**, 1713–1725.